

# Hector V3.2.0: functionality and performance of a reduced-complexity climate model

Kalyn Dorheim<sup>1</sup>, Skylar Gering<sup>2</sup>, Robert Gieseke<sup>3</sup>, Corinne Hartin<sup>4</sup>, Leeya Pressburger<sup>1</sup>, Alexey N. Shiklomanov<sup>5</sup>, Steven J. Smith<sup>1</sup>, Claudia Tebaldi<sup>1</sup>, Dawn Woodard<sup>1,6</sup>, Ben Bond-Lamberty<sup>1</sup>

1. University Joint Global Change Research Institute, Pacific Northwest National Laboratory, 5825 University Research Ct. #3500, College Park, MD 20740 USA
2. California Institute of Technology 1200 E California Blvd, Pasadena, CA 91125 USA
3. Independent Researcher, Potsdam, Germany
4. Climate Change Division, Office of Atmospheric Protection, U.S. Environmental Protection Agency, Washington, DC, USA
5. NASA Goddard Space Flight Center, 8800 Greenbelt Rd., Greenbelt, MD, 20771 USA
6. Natural Resources Defense Council, 1152 15th St NW #300, Washington, DC 20005 USA

*Correspondence to:* Kalyn Dorheim ([kalyn.dorheim@pnnl.gov](mailto:kalyn.dorheim@pnnl.gov))

**Abstract.** Hector is an open-source reduced complexity climate-carbon cycle model that models critical Earth system processes on a global and annual basis. Here we present an updated version of the model, Hector V3.2.0 (hereafter Hector V3) and document its new features, implementation of new science, and performance. Significant new features include permafrost thaw, a reworked energy balance submodel, and updated parameterizations throughout. Hector V3 results are in good general agreement with historical observations of atmospheric CO<sub>2</sub> concentrations and global mean surface temperature, and its future temperature projections are consistent with more complex Earth System Model output data from the Sixth Coupled Model Intercomparison Project. We show that Hector V3 is a fully open source, flexible, performant, and robust simulator of global climate changes, note its limitations, and discuss future areas of improvement and research with respect to the model’s scientific, stakeholder, and educational priorities.

## 1 Introduction

Reduced complexity climate models (RCMs) fill a critical role within the diverse climate modeling landscape (Sarofim et al., 2021). With strategically simpler representations of large-scale climate processes and dynamics in contrast to coupled Earth System Models (ESMs), RCMs are computationally efficient sources of future climate projections, able to produce large ensembles of results and explore key uncertainties at a fraction of the computational cost of a single ESM run (Kawamiya et

28 al., 2020). For this reason, RCMs such as Hector, MAGICC, FaIR, and the other Reduced Complexity Intercomparison  
29 Project (RCMIP) participating models (Nicholls et al., 2021; Meinshausen et al., 2011; Smith et al., 2018; Nicholls et al.,  
30 2020) have been coupled with socioeconomic models (Calvin et al., 2019); used to study climate-carbon interactions and  
31 feedbacks (Woodard et al., 2021); supported the assessment of key quantities like global temperature and the carbon budget  
32 in various Intergovernmental Panel on Climate Change (IPCC) reports (Smith et al., 2021; Forster et al., 2021); and other  
33 applications.

34

35 Hector is a globally resolved carbon-climate RCM with explicit terrestrial and ocean carbon cycles as well as active surface  
36 ocean chemistry. As a stand-alone climate model, Hector has been used in a variety of other research projects (Woodard et  
37 al., 2021; Dorheim et al., 2020; Schwarber et al., 2019; Vega-Westhoff et al., 2019; Pressburger et al., 2023) and participated  
38 in the first two phases of RCMIP (Nicholls et al., 2021, 2020). In addition, since 2015, Hector has been the climate  
39 component of the Global Change Analysis Model (GCAM) (Calvin et al., 2019) and used to explore the feedback from  
40 hydrofluorocarbon emissions from future changes in heating and cooling degree days (Hartin et al., 2021) as well as how  
41 carbon dioxide (CO<sub>2</sub>) removal technologies may impact the energy-water-land system (Fuhrman et al., 2023).

42

43 Since its initial release, model development of Hector has continued in order to reflect the advances made within the climate  
44 science and open-source software research communities, and the objective of this paper is to document the latest version of  
45 the model. We provide an overview of the model before describing the major changes and upgrades that have been made  
46 since Hector V1, focusing on the default model configuration but also describing optional settings. We then compare Hector  
47 V3 results with observations and ESM output to examine model performance, and finally discuss future areas of  
48 improvement for the model in the context of its goals of accuracy, performance, and broad accessibility.

## 49 **2 Methods**

### 50 **2.1 Model General Description**

51 The first version of Hector (V1) was described in detail by Hartin et al. (2015). It is a self-contained object-oriented model  
52 implemented in C++ with a modular, flexible design. While Hector produces annual output, its adaptive-time solver is  
53 capable of operating at a higher frequency to help address issues with numerical instability.

54

55 In its default configuration, all Hector runs begin after “spinup” (Thornton and Rosenbloom, 2005), in which the model runs  
56 until all carbon pools are in equilibrium; this typically requires ~300 years using the default model parametrization, and  
57 typically results in changes of a few percent in the model’s major carbon pools. After the spinup phase is complete, the main  
58 Hector run begins. A Hector run can either be “free-running” or “constrained.” By default, the model is free-running,  
59 meaning that its behavior is determined by the time series of emissions and other inputs. During a *constrained* run, the model

60 is forced to match one or more user-prescribed time series. The default free-running model uses time series from 37  
61 different emission species and 3 exogenous radiative forcers (see **Supplementary Tables 1**). These emission inputs fall into  
62 two categories. The first category consists of emissions that accumulate as greenhouse gas (GHG) concentrations. The GHG  
63 concentrations for nitrous oxide (N<sub>2</sub>O), methane (CH<sub>4</sub>), and 26 halocarbons are calculated using equations that encode a  
64 simplified relationship between emissions and concentrations (**Supplementary Tables 3-5**). The GHG concentrations for  
65 ozone (O<sub>3</sub>) are calculated from interactions between nitrogen oxides (NO<sub>x</sub>), carbon monoxide (CO), and non-methane  
66 volatile organic compound (NMVOC) emissions (Equations 42-43 in **Supplementary Table 9**). The atmospheric CO<sub>2</sub>  
67 concentrations are determined in part by the anthropogenic CO<sub>2</sub> emissions (read in as an input) and by the behavior of  
68 Hector's terrestrial and ocean carbon cycle components (**Figure 1**). The second category consists of the emissions that  
69 impact Hector's radiative forcing budget: carbon monoxide (CO), black carbon (BC), organic carbon (OC), sulfur dioxide  
70 (SO<sub>2</sub>), and ammonia (NH<sub>3</sub>). These emissions are used in equations (**Supplementary Information**) that determine aerosol  
71 concentrations and thus radiative forcings. The total radiative forcing is the sum of the forcing effects of all of Hector's  
72 atmospheric greenhouse gases, aerosols, and several additional forcing inputs (volcanic forcing, albedo).

73  
74 Total radiative forcing is then used to simulate temperature change. Hector's temperature component (Vega-Westhoff et al.,  
75 2019) is an implementation of the Diffusion Ocean Energy balance CLIMate model (Kriegler, 2005; Tanaka et al., 2007).  
76 DOECLIM is a 1-D pure diffusion ocean model that calculates changes in air temperature 2 meters over ocean/land, sea  
77 surface temperature, and within the ocean mixed layer. The sea surface and land surface temperatures from DOECLIM are  
78 used by Hector's ocean and land carbon cycles to calculate the carbon fluxes at the next time step. Hector's global mean  
79 surface temperature (GMST) is the area-weighted average of these land surface and ocean surface temperatures.

## 80 **2.2 Changes Since V1**

81 A number of significant architectural, software, and scientific developments have been implemented since the V1 release and  
82 documentation manuscript (Hartin et al., 2015). We start by documenting these software changes before discussing other  
83 changes and new features affecting Hector's carbon cycle, radiative forcing, temperature calculations, and constrained mode  
84 capabilities.

### 85 **2.2.1 Software**

86 Hector is an open-source community model available on GitHub (<https://github.com/jgcri/hector>). The repository includes  
87 updated project solutions and make files to support building and running Hector from the command line or development  
88 environments such as Visual Studio (<https://visualstudio.microsoft.com/>) or Xcode (<https://developer.apple.com/xcode/>).  
89 Alternatively, users can run Hector as an R (R Core Team, 2021) package, allowing for a broader range of users given R's  
90 popularity as a data analysis and simulation tool across many scientific disciplines. The R package wrapper enabled the

91 development of the Hector User Interface (Pennington and Vernon, 2021), which allows users to run and interact with  
92 Hector results in a web browser. Other changes include updated and reduced software dependencies, automated software  
93 testing, and auto-generated online documentation. Finally, a Python wrapper Pyhector (Willner et al., 2017) is maintained by  
94 community collaborators, broadening the potential users and use cases of the model. The default model remains highly  
95 performant: even without any speed optimizations at compile time, running the 550 years (1750-2300) of a standard run  
96 takes ~0.5s on a modern laptop. The model is also straightforward to parallelize for large-ensemble analyses (Pressburger et  
97 al., 2023). Ultimately, these Hector V3 software changes have led to a more robust, transparent, and accessible community  
98 model.

### 99 **2.2.2 Carbon Cycle**

100 Anthropogenic CO<sub>2</sub> emissions are debited from a geological pool (named “earth” in Hector; cf. **Figure 1**) pool and added to  
101 the one-pool, global atmosphere at each timestep. Hector’s active carbon cycle is split into terrestrial land and ocean  
102 submodels.

103  
104 As described in detail by Hartin et al. (2015, 2016), Hector’s ocean carbon cycle is a four-box module, consisting of two  
105 surface-level, intermediate, and deep ocean boxes (**Figure 1**). Carbon and water mass exchange occur between the four  
106 boxes respecting simplified representations of advection and thermohaline circulation, with volume transports tuned to  
107 approximate a flow of 100 Pg C from the surface high-latitude box to the deep ocean box at steady state, simulating deep  
108 water formation. Hector solves for the marine carbonate variables (DIC, pH, alkalinity) with respect to solubility in the two  
109 surface layer boxes (Zeebe and Wolf-Gladrow, 2001). The calculation of pCO<sub>2</sub> in each surface box is based on the  
110 concentration of CO<sub>2</sub> in the ocean and its solubility, in turn a function of temperature, salinity, and pressure. At steady state,  
111 the cold high-latitude surface box (> 55° N or S) acts as a sink of carbon from the atmosphere, while the warm low-latitude  
112 (≤ 55° N or S) surface box off-gases carbon back to the atmosphere. The ocean-atmosphere flux calculation follows  
113 Takahashi et al. (2009). In Hector V3, ocean carbon cycle calculations use sea surface temperature (SST) calculated by  
114 DOECLIM (see above), and the preindustrial surface and intermediate/deep ocean carbon cycle pools are initialised from the  
115 IPCC sixth assessment report (AR6) Figure 5.12 (Canadell et al., 2021) (see **Table 1**).

116  
117 Much of the basic functionality of the model’s terrestrial carbon cycle is unchanged from the original V1 release (Hartin et  
118 al., 2015). Net primary production (NPP) is partitioned into vegetation, detritus, and soil (Figure 1); litterfall moves carbon  
119 from vegetation to the soil, and temperature-dependent, first-order decay equations control the heterotrophic release of CO<sub>2</sub>  
120 back to the atmosphere from the latter two pools (Hartin et al., 2015). By default, the terrestrial carbon cycle operates as a  
121 single, global biome, but Hector can run with an arbitrary number of independent biomes, each with its own set of carbon

122 pools and parameters; a sample multi-biome parameterization is included with the model's input files, and an example of this  
123 was documented in detail by Woodard et al. (2021).

124

125 There are also new or changed behaviors in the Hector V3 terrestrial carbon submodel. First, previously land use change  
126 (LUC) emissions were specified as a single time series that could be positive or negative, reflecting net emission or uptake,  
127 and this value was added (subtracted) to the atmosphere and subtracted (added) from the vegetation, detritus, and soil pools  
128 (Hartin et al., 2015). In V3, these are now provided in separate input time series that must be strictly positive and correspond  
129 to the gross emissions and uptake fluxes, respectively, and because of how LUC now affects NPP (see below), are assumed  
130 to include any regrowth fluxes from previous LUC. A similar change has been made to the fossil fuel/industrial emissions,  
131 which are now specified by two gross fluxes of emissions and uptake. This provides users with more flexibility to specify  
132 how the gross fluxes result in the net flux, but no behavior change otherwise. Note that the model still accepts net fluxes if  
133 that is all that is available, as is the case for the RCMIP Shared Socioeconomic Pathway (SSP) scenarios (Nicholls et al.,  
134 2020).

135

136 Second, LUC fluxes now affect the land carbon pools in proportion to those pools' size, not via fixed allocation fractions as  
137 previously. This is a more conservative assumption than the previous user-defined allocation approach, given the large  
138 uncertainty about LUC flux magnitudes and interactive carbon-cycle effects (Yue et al., 2020; Friedlingstein et al., 2023). In  
139 addition, in a non-spatial model such as Hector, the carbon pool sizes are governed by the total amount of carbon in the  
140 system and the first-order equations linking the pools; LUC loss is only temporary until the pools re-equilibrate. The new  
141 approach is thus simpler and in most cases will have only minor effects on model results.

142

143 Third, terrestrial NPP is now affected by LUC: the model tracks how much cumulative carbon has been lost (or gained) due  
144 to LUC, relative to preindustrial conditions, and then adjusts NPP by this fraction in addition to the pre-existing temperature  
145 and CO<sub>2</sub> adjustments to NPP described by Hartin et al. (2015). The logic behind this change is that extensive historical  
146 deforestation is known to affect photosynthesis and NPP (Ito, 2011; Malhi et al., 2004; Kaplan et al., 2012), and in previous  
147 versions of Hector deforestation did not affect the model's NPP at all. The new behavior is:

$$NPP(t) = NPP_0 \times f(C_{atm}, \beta) \times f(LUC_v) \quad (1)$$

148 where  $t$  is the current timestep;  $NPP_0$  is pre-industrial NPP; and the two  $f$  terms represent CO<sub>2</sub> fertilization (Wang et al.,  
149 2020) and the aforementioned LUC effect on NPP. This change provides a better match with known LUC effects on  
150 terrestrial biomass and production (Winkler et al., 2021; Malhi et al., 2004). More generally, it means that Hector does not  
151 regrow vegetation after LUC-driven deforestation; regrowth fluxes should be included in the LUC inputs (see above).

152

153 Fourth, Hector V3 also includes a novel implementation of permafrost thaw, a potentially significant process affecting the  
154 earth system (Hugelius et al., 2020) that releases both CO<sub>2</sub> and CH<sub>4</sub> into the atmosphere. Hector’s permafrost  
155 implementation was fully described by Woodard et al. (2021). Briefly, permafrost is treated as a separate land carbon pool  
156 that becomes available for decomposition into both CH<sub>4</sub> and CO<sub>2</sub> once thawed (Schädel et al., 2014). The thaw rate is  
157 controlled by biome-specific land surface temperature and calibrated to be consistent with both historical data and CMIP6  
158 projections (Burke et al., 2020). Woodard et al. (2021) found that the fraction of thawed permafrost carbon available for  
159 decomposition was the most influential parameter in this approach and that adding permafrost thaw to Hector resulted in  
160 0.2–0.25 °C of additional warming over the 21<sup>st</sup> century. The addition of permafrost to the V3 model produced changes in  
161 climate and permafrost carbon pools fully consistent with those reported by Woodard et al (2021).

162  
163 An optional new feature in Hector V3 is the ability to track the flow of carbon as it moves between the land and ocean  
164 carbon pools and the atmosphere (as CO<sub>2</sub>). At a user-defined start-tracking date, the model tags all carbon in each of its pools  
165 as self-originating—e.g., the soil pool is deemed to be composed of 100% soil-origin carbon. As the model then runs  
166 forward, the origin tag is retained as carbon is exchanged between the models’ various pools; if 1 Pg C with origin X is  
167 incorporated into a 19 Pg C pool with origin Y, for example, at the next timestep, the 20 Pg C pool is tracked as 5% origin X,  
168 95% origin Y. At the end of a run, detailed information about the composition of each pool at each time point can be  
169 analyzed. This capability does not affect model behavior or any outputs, although it does impose a substantial performance  
170 penalty. Carbon tracking was described in detail by Pressburger et al. (2023) and is off by default.

### 171 **2.2.3 Radiative Forcing**

172 At each time step, after Hector’s carbon cycle solves and all GHG concentrations are computed, Hector calculates total  
173 radiative forcing as the sum of 39 forcing effects (listed in **Supplementary Table 1**), each relative to the 1750 base year.  
174 The forcing effects for volcanoes and albedo are read in as inputs, as well as a normally-unused “miscellaneous forcing”  
175 input available for experimental manipulation. The remaining 36 forcing effects for various aerosols, aerosol-cloud  
176 interactions, pollutants, and greenhouse gases are calculated internally within Hector. The forcing effects of tropospheric O<sub>3</sub>  
177 and stratospheric H<sub>2</sub>O use the same calculations as Hartin et al. (2015). For the other forcing agents, CO<sub>2</sub>, CH<sub>4</sub>, N<sub>2</sub>O, 26  
178 halocarbons, aerosol-cloud interactions, and effects of BC, OC, SO<sub>2</sub>, and NH<sub>3</sub>, Hector V3 has adopted the forcing equations  
179 from AR6 (see **Supplementary Table 5**). Of these, the forcing effect from NH<sub>3</sub> was not previously included in Hector. In  
180 addition, the aerosol-cloud interaction forcing replaces the indirect effects of SO<sub>2</sub> forcing that was previously used to  
181 approximate the SO<sub>2</sub> and cloud interactions.

## 182 2.2.4 Temperature

183 As of V2, Hector replaced a 0-D energy balance model with DOECLIM (Vega-Westhoff et al., 2019). DOECLIM uses  
184 Hector’s total radiative forcing to determine global temperature change. DOECLIM is a four-box energy balance model,  
185 meaning that it models heat transfer within the climate system represented by four idealized boxes: land (surface), air (2  
186 meters) over land, air (2 meters) over the ocean, and sea surface (ocean mixed layer). DOECLIM uses a system of  
187 differential equations to model the temperature change in the four boxes in response to radiative forcing while accounting for  
188 the proportional differences in ocean and land masses and effective heat capacity (Tanaka et al., 2007).

189  
190 In Hector V3, DOECLIM is a fully integrated component of the model, and its outputs now affect Hector’s land carbon  
191 cycle: DOECLIM’s land temperature drives heterotrophic respiration, and sea surface temperature affects ocean carbon cycle  
192 dynamics. The difference in land and ocean temperature change, or land-ocean warming ratio, is an emergent property of  
193 DOECLIM and is used by default. Two additional parameters can be used to adjust the contributions of aerosols (BC, OC,  
194 SO<sub>2</sub>, NH<sub>3</sub>, and aerosol-cloud interactions) and volcanic forcing to global temperature. By default these are set to a value of  
195 one, with the assumption being that the forcing-temperature relationship is consistent for all forcers. These scalar terms  
196 allow users to adjust the temperature sensitivity to aerosol and volcanic forcing in uncertainty analyses or when using Hector  
197 to emulate ESMs that exhibit different sensitivities to aerosol and volcanic forcings (Dorheim et al. 2020).

## 198 2.2.5 Constraints

199 Hector can run in a “constrained” mode that allows users to overwrite a specified Hector variable with a prescribed time  
200 series. Values can be prescribed for atmospheric CO<sub>2</sub> and all other GHG concentrations (effectively resulting in a  
201 concentration-forced, not emissions-forced, run). In addition, global temperature, total radiative forcing, and net biome  
202 production (effectively turning off the model’s terrestrial carbon cycle) can also be constrained. When running in the  
203 constrained mode, user-provided values seamlessly overwrite internally-calculated ones, and thus will be used by the  
204 downstream Hector components. For example, a Hector run that uses the total total radiative forcing constraint will use the  
205 user-prescribed values to calculate energy fluxes and temperature change instead of Hector’s internally calculated total ones  
206 (see **Table 2** for more examples and details).

207  
208 The ability to run in the constrained mode is a useful feature that has a number of applications. For example, Hector’s  
209 concentration constraints enable concentration-forced experiments (e.g., 1% CO<sub>2</sub> and abrupt 4 x CO<sub>2</sub> (Eyring et al., 2016) to  
210 comply with the RCMIP protocol (Nicholls et al., 2020). In addition, constraints facilitate coupling Hector with other  
211 models: the Net Biome Production (NBP) constraint can be used to pass global NBP value from a regional terrestrial carbon  
212 cycle model to Hector, and from there, Hector’s ocean carbon cycle and climate dynamics will be calculated. Finally,  
213 running Hector in constrained mode can help diagnose model behavior. For example, concentration constraints can be used

214 after a new model development leads to an unexpected increase in global temperature. Running Hector with constrained CO<sub>2</sub>  
215 concentrations or with total RF will help the developer attribute this novel behavior to changes to Hector's carbon cycle or  
216 climate dynamics.

## 217 **2.2.6 Model Parameterization**

218 Hector's V3 default parameterization is mostly inherited from previous versions of Hector (Hartin et al., 2015; Vega-Westhoff  
219 et al., 2019), with the exception of when robust updated estimates are available. In particular, the V3 model uses more recent  
220 estimates published for pre-industrial NPP, CO<sub>2</sub>, CH<sub>4</sub>, and N<sub>2</sub>O concentrations, as well as estimates of the pre-industrial carbon  
221 cycle to initialize its ocean carbon pools (**Table 1**). Initial pre-industrial sea surface temperatures used by Hector's ocean  
222 component were updated from a CMIP5 multi-model mean to a CMIP6 multi-model mean. Historical ocean surface  
223 temperature output files from 24 CMIP6 participating models (see **Supplementary Table 10**) were processed to compute the  
224 area-weighted mean temperature globally, at both high (> 55°) and low (≤ 55°) latitudes from 1850 to 1860 (**Table 1**).

225  
226 To calibrate the final model, five additional Hector parameters were fit to comparison data using a Nelder-Mead  
227 optimization routine (Nelder and Mead, 1965) in a two-part protocol. First, the natural N<sub>2</sub>O and CH<sub>4</sub> emissions, which are  
228 assumed to be constant throughout the run, were calibrated to median AR6 N<sub>2</sub>O and CH<sub>4</sub> radiative forcing (Smith et al.,  
229 2018). Second, three Hector parameters—the CO<sub>2</sub> fertilization factor  $\beta$  (unitless), heterotrophic respiration temperature  
230 sensitivity  $Q_{10}$  (unitless), and ocean heat diffusivity  $\kappa$  (cm<sup>2</sup> s<sup>-1</sup>)—were fit to historic CO<sub>2</sub> concentrations (Meinshausen et al.,  
231 2017) and GMST (Morice et al., 2021) observations from 1850 to 2021. The Meinshausen et al. (2017) records consist of  
232 data for a single year in 1750 and then a complete time series from 1850 to 2014. We chose to use CO<sub>2</sub> and GMST because  
233 they are observed data with long time series; conversely, other potential records such as ocean and land sink estimates come  
234 from either inversions or models (Friedlingstein et al., 2023). The optimization routine simultaneously minimized the  
235 average of the two variables' mean squared errors between Hector CO<sub>2</sub> concentrations and GMST and these observed data.  
236 Parameter bounds (i.e., beyond which the optimizer was not allowed) were set at  $\pm 2\sigma$ , i.e. for a normally-distributed variable  
237 ~95% of the possible distribution was used. The best fits for  $\beta$ ,  $Q_{10}$ , and  $\kappa$  (**Table 1**) were then set as Hector V3's default  
238 parameters. The materials and scripts used to calibrate Hector are available in the manuscript repository  
239 ([https://github.com/JGCRI/Dorheim\\_etal\\_2024\\_GMD](https://github.com/JGCRI/Dorheim_etal_2024_GMD)) to ensure the reproducibility and transparency of the calibration  
240 process.

## 241 **2.3 Model runs and analysis**

242 To assess model performance, we compared Hector results with both observations and ESM projections. For the historical  
243 period, we ran Hector in its default emission-driven mode, with inputs according to the RCMIP protocol (Nicholls et al.,  
244 2021, 2020) and the default parameterization described in the previous section. Hector's GMST results from 1850 to 2021



245 were compared with HadCRUT5 (Morice et al., 2021) GMST observations, while Hector's CO<sub>2</sub> concentrations in the year  
246 1750, and then from 1850 to 2014, were compared with the CMIP6 (Meinshausen et al., 2017) CO<sub>2</sub> concentrations. We used  
247 root mean squared error (RMSE) to quantify the differences between model results and the observations. An ordinary least  
248 squares linear regression was fit to Hector results and the observational data products to provide additional insights into the  
249 goodness of fit. An R<sup>2</sup> value close to one suggests a high degree of correlation between the Hector results and the  
250 observations.

251

252 For the future period, we first compared Hector's temperature with the AR6 near-term (2021-2024), mid-term (2041-2060),  
253 and long-term (2081-2100) warming. For this, Hector was run in emissions-driven mode using the emissions from the  
254 RCMIP (Nicholls et al., 2020) protocol. Hector's near-term, mid-term, and long-term warming were computed as the 20-  
255 year averages using the model's global mean surface temperature output.

256

257 Second, the model was run in a *constrained mode*, in which concentrations for CO<sub>2</sub>, CH<sub>4</sub>, N<sub>2</sub>O, and 26 halocarbons from  
258 RCMIP (Nicholls et al., 2020) were prescribed, and compared with CMIP6. These concentration-driven runs were consistent  
259 with the CMIP6 protocol (Eyring et al., 2016), allowing for a direct comparison of Hector's climate dynamics with that of  
260 the ESMs. For this step, output files from 15 ESMs were processed to compute area-weighted global air, land air, and sea  
261 surface temperature anomalies. The CMIP6 models were selected based on data availability for the variables and scenarios; a  
262 complete list of models is given in **Supplementary Table 11**. We used the first available ensemble member, since the  
263 internal variability between members was unlikely to affect long-term dynamics that are the focus of RCMs (Eyring et al.,  
264 2016).

### 265 **3 Results & Discussion**

266 Hector's historical CO<sub>2</sub> concentrations from an emission-driven run are compared with the Meinshausen et al. (2017) dataset  
267 in **Figure 2**. The Hector results closely follow the observed values with a RMSE of 2.14 ppm CO<sub>2</sub> and a correlation  
268 coefficient of 0.99, indicating a good agreement between Hector's output and historical carbon cycle observations. **Figure 3**  
269 compares emission-driven Hector global mean temperature with historical observations (Morice et al., 2021). The difference  
270 between Hector's results and observations is an RMSE of 0.18 °C, which is less than the 0.36 °C standard deviation of the  
271 comparison dataset. The linear fit between Hector results and observations has an adjusted R<sup>2</sup> value of 0.87 (**Figure 3**). The  
272 recent (2012-2021) decadal average global mean surface temperature for Hector was 0.75 ± 0.09 °C. The model's most  
273 notable departure from the observational record is in the late 19<sup>th</sup> and early 20<sup>th</sup> centuries (Bauer et al., 2020; Nicholls et al.,  
274 2020). The model also generally reproduces modern-day airborne fraction values (Jones et al., 2013; Pressburger et al.,  
275 2023). The model's modern (2014-2024) decadal average sea surface temperature and ocean pH are 0.78 ± 0.08 °C and 8.1  
276 ± 0.008, respectively. Hector's land sink for 2013-2022 was 1.94 ± 0.1 Pg C yr<sup>-1</sup>, which is lower than the land sink of

277  $2.9 \pm 0.9 \text{ Pg C yr}^{-1}$  reported by the Global Carbon Project (GCP, Friedlingstein et al., 2023) during the same decade.  
278 Hector's ocean sink of  $3.08 \pm 0.13 \text{ Pg C yr}^{-1}$  is consistent with the GCP ocean sink of  $2.8 \pm 0.4 \text{ Pg C yr}^{-1}$ . Ultimately, we  
279 conclude that emission-driven Hector results are in agreement with historical temperature and  $\text{CO}_2$  observations except, as  
280 noted above, for the latter half of the 19<sup>th</sup> century.

281  
282 The comparison of Hector's historical results with observations is complemented by evaluating Hector's future temperature  
283 results against CMIP6 (**Figure 4**) and AR6 assessed warming (Canadell et al., 2021). For the future SSP1-2.6, SSP2-4.5, and  
284 SSP5-8.5 projections, Hector's temperature outputs fall squarely within the CMIP6 model spread (**Figure 4**). In addition,  
285 **Figure 5** shows Hector's performance in two stylized experiments, 1% $\text{CO}_2$  and 4x $\text{CO}_2$  relative to CMIP6 ESMs. These are  
286 baseline experiments of the CMIP DECK protocol (Eyring et al., 2016) designed to diagnose a model's climate sensitivity,  
287 feedback strength, provide an idealized benchmark for its transient behavior (for 1% $\text{CO}_2$ ); and characterize its climate  
288 sensitivity and fast-response performance (for 4x $\text{CO}_2$ ). Again the model falls squarely within the CMIP6 model spread, with  
289 no suggestion of anomalous behavior. Hector's transient climate response to cumulative  $\text{CO}_2$  emissions is  $1.51 \text{ }^\circ\text{C per 1000}$   
290  $\text{Pg C}$ , which is cooler than the IPCC AR6 assessed best estimate of  $1.65 \text{ }^\circ\text{C per 1000 Pg C}$  but falls within the "very likely"  
291 range of  $1.0$  to  $2.3 \text{ }^\circ\text{C per 1000 Pg C}$  (Arias et al., 2021). In general, we conclude that the model exhibits climate responses  
292 consistent with AR6 (**Table 3**).

## 293 **4 Conclusions**

294 In this manuscript, we documented the changes and new features of Hector V3. We showed that emissions-driven Hector's  
295 historical results are generally consistent with observed  $\text{CO}_2$  concentrations and global mean surface temperature, with the  
296 exception of late 19<sup>th</sup> and early 20<sup>th</sup> century cooling (Bauer et al., 2020). Hector's future projections of land, ocean, and  
297 global average temperature are consistent with a CMIP6 ensemble of models. Thus, we conclude that in the context of  
298 RCMs, Hector reproduces most global-scale historical trends and outputs 21<sup>st</sup>-century projections consistent with Earth  
299 system models.

300  
301 This fidelity to the current climate and future CMIP6 projections means that there are many potential use cases for Hector,  
302 but it is important for users to understand the advantages (as well as disadvantages) in using it relative to other RCMs or  
303 ESMs (Nicholls et al., 2021). The freely available R package and online interface facilitate its integration into both standard  
304 analytical pipelines as well classroom settings so that students can get hands-on experience with running a climate model and  
305 interpreting results; such educational use is supported by the fact that Hector is a well-documented open-source climate  
306 model with multiple means of running the model (Hector UI, R Hector, and C++ executable). The model's fully open-source  
307 C++ core is easy to couple with other models (Calvin et al., 2019). Using the Hector R package  
308 (<https://github.com/jgcri/hector>), it is easy to generate and analyze large ensembles of Hector results which can be used to

309 explore uncertainty spaces (Nicholls et al., 2021; Pressburger et al., 2023). Finally, Hector’s performance and open, flexible  
310 calibration procedure support efforts to emulate more-complex ESMs in support of novel, computationally-intensive  
311 experiments (Lu and Ricciuto, 2019; Chen et al., 2023).

312

313 It is also important to note Hector’s limitations. The model is more complex and thus harder to understand than approaches  
314 such as FAIR (Leach et al., 2021), although comparable in complexity to MAGICC (Meinshausen et al., 2011). Hector does  
315 not account for the ocean biological pump or changes in ocean stratification; whether these errors are compensating or  
316 compounding is unclear and merits future research (Jin et al., 2020). Longer-term simulations are outside of Hector’s scope,  
317 as is true of most RCMs, as the model’s ocean does not include the heat storage changes that strongly affect long-term global  
318 temperature dynamics (Baggenstos et al., 2019; Abraham et al., 2013). Future work should aim at understanding/rectifying  
319 the differences between Hector’s terrestrial carbon sink and other sources while remaining consistent with Hector’s moderate  
320 complexity and goals; it will always be important to consider trade-offs between costs (i.e., increased complexity threatening  
321 interpretability; increased predictive uncertainty from additional model parameters; computational efficiency) and benefits  
322 (increased fidelity and representativeness) (Sarofim et al., 2021).

323

324 Finally, in addition to continued science improvements, future versions of Hector will benefit from added infrastructure  
325 capabilities. First, the current parameter-calibration routine is relatively simple and it may be worth exploring more  
326 sophisticated model-calibration procedures (Chen et al., 2023) in future versions of Hector. In addition, a turnkey ability to  
327 do probabilistic model forecasts (Fawcett et al., 2015; Ou et al., 2021), i.e. propagating parameter distributions and  
328 uncertainty (Pressburger et al., 2023) to produce probabilities of future climate change, is an important capability that a  
329 companion R package has been developed to handle (Brown et al., 2024). Leveraging this new capability for probabilistic  
330 projects will be important for future analyses using Hector to understand the changing earth and climate system.

331 **Code Availability:** Hector V3.2.0 was used to generate the Hector results analyzed and used to generate the figures included  
332 in the main text and in the supplementary information. This version of Hector is available at  
333 <https://github.com/JGCRI/hector> at the V3.2.0 release and is archived at <https://zenodo.org/records/10698028> this includes  
334 all the initialization, emission, and concentration files. All of the code and data used to calibrate Hector, perform all model  
335 runs, and produce data visualisations are available at [https://github.com/JGCRI/Dorheim\\_etal\\_2024\\_GMD](https://github.com/JGCRI/Dorheim_etal_2024_GMD) and the GMD3  
336 release associated with this iteration of the manuscript is archived at <https://zenodo.org/records/10698650>.

337 **Data Availability:** All of the calibration, comparison data, and Hector results, along with scripts used to prepare Hector runs  
338 analyzed and used to generate the figures included in the main text and in the supplementary information, are available at

339 [https://github.com/JGCRI/Dorheim\\_etal\\_2024\\_GMD](https://github.com/JGCRI/Dorheim_etal_2024_GMD) specifically release GMD3 archived at zendo  
340 <https://zenodo.org/records/10698650> is the release associated with this iteration of the manuscript.

341 **Author contribution:** KD, BB, SS, SK, RG, CH, LP, AS, and DW all contributed to Hector development. CT and SS  
342 helped conceptualize model experiments. KD and BB led the preparation of the original draft and all coauthors contributed  
343 to the final draft.

344 **Competing interests:** The authors declare that they have no conflict of interest.

345 **Disclaimer:** The views expressed in this article are those of the authors and do not necessarily represent the views or policies  
346 of the U.S. Department of Energy, Environmental Protection Agency, or National Aeronautics and Space Administration.

347 **Acknowledgments:** This research was supported by the U.S. Department of Energy, Office of Science, as part of research in  
348 MultiSector Dynamics, Earth and Environmental System Modeling Program. The authors would also like to acknowledge  
349 EPA Project DW-089-92459801-8 for contributing to the radiative forcing updates including in Hector v3. The authors  
350 would also like to acknowledge Robert Link and Sven Willner for their contributions to Hector and work on R Hector and  
351 Py Hector, respectively.

## 352 **References**

- 353 Abraham, J. P., Baringer, M., Bindoff, N. L., Boyer, T., Cheng, L. J., Church, J. A., Conroy, J. L., Domingues, C. M., Fasullo, J. T.,  
354 Gilson, J., Goni, G., Good, S. A., Gorman, J. M., Gouretski, V., Ishii, M., Johnson, G. C., Kizu, S., Lyman, J. M., Macdonald, A. M.,  
355 Minkowycz, W. J., Moffitt, S. E., Palmer, M. D., Piola, A. R., Reseghetti, F., Schuckmann, K., Trenberth, K. E., Velicogna, I., and Willis,  
356 J. K.: A review of global ocean temperature observations: Implications for ocean heat content estimates and climate change, *Rev.*  
357 *Geophys.*, 51, 450–483, 2013.
- 358 Arias, P. A., Bellouin, N., Coppola, E., Jones, R. G., Krinner, G., Marotzke, J., Naik, V., Palmer, M. D., Plattner, G.-K., Rogelj, J., Rojas,  
359 M., Sillmann, J., Storelvmo, T., Thorne, P. W., Trewin, B., Achuta Rao, K., Adhikary, B., Allan, R. P., Armour, K., Bala, G., Barimalala,  
360 R., Berger, S., Canadell, J. G., Cassou, C., Cherchi, A., Collins, W., Collins, W. D., Connors, S. L., Corti, S., Cruz, F., Dentener, F. J.,  
361 Dereczynski, C., Di Luca, A., Diongue Niang, A., Doblus-Reyes, F. J., Dosio, A., Douville, H., Engelbrecht, F., Eyring, V., Fischer, E.,  
362 Forster, P., Fox-Kemper, B., Fuglested, J. S., Fyfe, J. C., Gillett, N. P., Goldfarb, L., Gorodetskaya, I., Gutierrez, J. M., Hamdi, R.,  
363 Hawkins, E., Hewitt, H. T., Hope, P., Islam, A. S., Jones, C., Kaufman, D. S., Kopp, R. E., Kosaka, Y., Kossin, J., Krakovska, S., Lee, J.-  
364 Y., Li, J., Mauritsen, T., Maycock, T. K., Meinshausen, M., Min, S.-K., Monteiro, P. M. S., Ngo-Duc, T., Otto, F., Pinto, I., Pirani, A.,  
365 Raghavan, K., Ranasinghe, R., Ruane, A. C., Ruiz, L., Sallée, J.-B., Samset, B. H., Sathyendranath, S., Seneviratne, S. I., Sörensson, A.  
366 A., Szopa, S., Takayabu, I., Tréguier, A.-M., van den Hurk, B., Vautard, R., von Schuckmann, K., Zaehle, S., Zhang, X., and Zickfeld, K.:  
367 Technical Summary, in: *Climate Change 2021: The Physical Science Basis. Contribution of Working Group I to the Sixth Assessment*  
368 *Report of the Intergovernmental Panel on Climate Change*, edited by: Masson-Delmotte, V., Zhai, P., Pirani, A., Connors, S. L., Péan, C.,  
369 Berger, S., Caud, N., Chen, Y., Goldfarb, L., Gomis, M. I., Huang, M., Leitzell, K., Lonnoy, E., Matthews, J. B. R., Maycock, T. K.,  
370 Waterfield, T., Yelekçi, O., Yu, R., and Zhou, B., Cambridge University Press, Cambridge, United Kingdom and New York, NY, USA,  
371 33–144, 2021.
- 372 Baggénstos, D., Häberli, M., Schmitt, J., Shackleton, S. A., Birner, B., Severinghaus, J. P., Kellerhals, T., and Fischer, H.: Earth’s radiative  
373 imbalance from the Last Glacial Maximum to the present, *Proceedings of the National Academy of Sciences*, 116, 14881–14886, 2019.
- 374 Bauer, S. E., Tsigaridis, K., Faluvegi, G., Kelley, M., Lo, K. K., Miller, R. L., Nazarenko, L., Schmidt, G. A., and Wu, J.: Historical

- 375 (1850–2014) aerosol evolution and role on climate forcing using the GISS ModelE2.1 contribution to CMIP6, *J. Adv. Model. Earth Syst.*,  
376 12, <https://doi.org/10.1029/2019ms001978>, 2020.
- 377 Brown, J., Smith, S., Tebaldi, C., Pressburger, L., Dorheim, K., and Bond-Lamberty, B.: Matilda v1.0: An R package for probabilistic  
378 climate projections using a reduced complexity climate model, *PLOS Climate*, in press, 2024.
- 379 Burke, E. J., Zhang, Y., and Krinner, G.: Evaluating permafrost physics in the Coupled Model Intercomparison Project 6 (CMIP6) models  
380 and their sensitivity to climate change, *Cryosphere*, 14, 3155–3174, 2020.
- 381 Calvin, K., Patel, P., Clarke, L., Asrar, G., Bond-Lamberty, B., Cui, R. Y., Vittorio, A. D., Dorheim, K., Edmonds, J., Hartin, C., and  
382 Others: GCAM v5. 1: representing the linkages between energy, water, land, climate, and economic systems, *Geoscientific Model  
383 Development*, 12, 677–698, 2019.
- 384 Canadell, J. G., Monteiro, P. M. S., Costa, M. H., Cotrim da Cunha, L., Cox, P. M., Eliseev, A. V., Henson, S., Ishii, M., Jaccard, S.,  
385 Koven, C., Lohila, A., Patra, P. K., Piao, S., Rogelj, J., Syampungani, S., Zaehle, S., and Zickfeld, K.: Global Carbon and other  
386 Biogeochemical Cycles and Feedbacks, in: *Climate Change 2021: The Physical Science Basis. Contribution of Working Group I to the  
387 Sixth Assessment Report of the Intergovernmental Panel on Climate Change*, edited by: Masson-Delmotte, V., Zhai, P., Pirani, A.,  
388 Connors, S. L., Péan, C., Berger, S., Caud, N., Chen, Y., Goldfarb, L., Gomis, M. I., Huang, M., Leitzell, K., Lonnoy, E., Matthews, J. B.  
389 R., Maycock, T. K., Waterfield, T., Yelekçi, O., Yu, R., and Zhou, B., Cambridge University Press, Cambridge, United Kingdom and New  
390 York, NY, USA, 673–816, 2021.
- 391 Chen, M., Qian, Z., Boers, N., Jakeman, A. J., Kettner, A. J., Brandt, M., Kwan, M.-P., Batty, M., Li, W., Zhu, R., Luo, W., Ames, D. P.,  
392 Barton, C. M., Cuddy, S. M., Koirala, S., Zhang, F., Ratti, C., Liu, J., Zhong, T., Liu, J., Wen, Y., Yue, S., Zhu, Z., Zhang, Z., Sun, Z., Lin,  
393 J., Ma, Z., He, Y., Xu, K., Zhang, C., Lin, H., and Lü, G.: Iterative integration of deep learning in hybrid Earth surface system modelling,  
394 *Nature Reviews Earth & Environment*, 4, 568–581, 2023.
- 395 Dorheim, K., Link, R., Hartin, C., Kravitz, B., and Snyder, A.: Calibrating Simple Climate Models to Individual Earth System Models:  
396 Lessons Learned From Calibrating Hector, *Life Support Biosph. Sci.*, 7, e2019EA000980, 2020.
- 397 Eyring, V., Bony, S., Meehl, G. A., Senior, C. A., Stevens, B., Stouffer, R. J., and Taylor, K. E.: Overview of the Coupled Model  
398 Intercomparison Project Phase 6 (CMIP6) experimental design and organization, *Geosci. Model Dev.*, 9, 1937–1958, 2016.
- 399 Fawcett, A. A., Iyer, G. C., Clarke, L. E., Edmonds, J. A., Hultman, N. E., McJeon, H. C., Rogelj, J., Schuler, R., Alsalam, J., Asrar, G. R.,  
400 Creason, J., Jeong, M., McFarland, J., Mundra, A., and Shi, W.: CLIMATE POLICY. Can Paris pledges avert severe climate change?,  
401 *Science*, 350, 1168–1169, 2015.
- 402 Forster, P., Storelvmo, T., Armour, K., Collins, W., Dufresne, J.-L., Frame, D., Lunt, D. J., Mauritsen, T., Palmer, M. D., Watanabe, M.,  
403 Wild, M., and Zhang, H.: The Earth's Energy Budget, Climate Feedbacks, and Climate Sensitivity, in: *Climate Change 2021: The Physical  
404 Science Basis. Contribution of Working Group I to the Sixth Assessment Report of the Intergovernmental Panel on Climate Change*,  
405 edited by: Masson-Delmotte, V., Zhai, P., Pirani, A., Connors, S. L., Péan, C., Berger, S., Caud, N., Chen, Y., Goldfarb, L., Gomis, M. I.,  
406 Huang, M., Leitzell, K., Lonnoy, E., Matthews, J. B. R., Maycock, T. K., Waterfield, T., Yelekçi, O., Yu, R., and Zhou, B., Cambridge  
407 University Press, Cambridge, United Kingdom and New York, NY, USA, 923–1054, 2021.
- 408 Friedlingstein, P., Jones, M. W., Andrew, R. M., Bakker, D. C. E., Hauck, J., Landschützer, P., Le Quéré, C., Luijkx, I. T., Peters, G. P.,  
409 Peters, W., Pongratz, J., Schwingshackl, C., Sitch, S., Canadell, J. G., Ciais, P., Jackson, R. B., Alin, S. R., Anthoni, P., Barbero, L., Bates,  
410 N. R., Becker, M., Bellouin, N., Decharme, B., Bopp, L., Brasika, I. B. M., Cadule, P., Chamberlain, M. A., Chandra, N., Chau, T.-T.-T.,  
411 Chevallier, F., Chini, L. P., Cronin, M., Dou, X., Enyo, K., Evans, W., Falk, S., Feely, R. A., Feng, L., Ford, D. J., Gasser, T., Ghattas, J.,  
412 Gkritzalis, T., Grassi, G., Gregor, L., Gruber, N., Gürses, Ö., Harris, I., Hefner, M., Heinke, J., Houghton, R. A., Hurtt, G. C., Iida, Y.,  
413 Ilyina, T., Jacobson, A. R., Jain, A., Jarníková, T., Jersild, A., Jiang, F., Jin, Z., Joos, F., Kato, E., Keeling, R. F., Kennedy, D., Klein  
414 Goldewijk, K., Knauer, J., Korsbakken, J. I., Körtzinger, A., Lan, X., Lefèvre, N., Li, H., Liu, J., Liu, Z., Ma, L., Marland, G., Mayot, N.,  
415 McGuire, P. C., McKinley, G. A., Meyer, G., Morgan, E. J., Munro, D. R., Nakaoka, S.-I., Niwa, Y., Olsen, A., Omar, A. M., Ono, T.,  
416 Paulsen, M., Pierrot, D., Pocock, K., Poulter, B., Powis, C. M., Rehder, G., Resplandy, L., Robertson, E., Rödenbeck, C., Rosan, T. M.,  
417 Schwinger, J., Séférian, R., Smallman, T. L., Smith, S. M., et al.: Global Carbon Budget 2023, *Earth System Science Data*, 15, 5301–5369,  
418 2023.
- 419 Fuhrman, J., Bergero, C., Weber, M., Monteith, S., Wang, F. M., Clarens, A. F., Doney, S. C., Shobe, W., and McJeon, H.: Diverse carbon  
420 dioxide removal approaches could reduce impacts on the energy–water–land system, *Nat. Clim. Chang.*, 13, 341–350, 2023.

- 421 Hartin, C., Link, R., Patel, P., Mundra, A., Horowitz, R., Dorheim, K., and Clarke, L.: Integrated modeling of human-earth system  
422 interactions: An application of GCAM-fusion, *Energy Econ.*, 103, 105566, 2021.
- 423 Hartin, C. A., Patel, P., Schwarber, A., Link, R. P., and Bond-Lamberty, B. P.: A simple object-oriented and open-source model for  
424 scientific and policy analyses of the global climate system – Hector v1.0, *Geoscientific Model Development*, 8, 939–955, 2015.
- 425 Hartin, C. A., Bond-Lamberty, B., Patel, P., and Mundra, A.: Ocean acidification over the next three centuries using a simple global  
426 climate carbon-cycle model: projections and sensitivities, *Biogeosciences*, 4329–4342, 2016.
- 427 Hugelius, G., Loisel, J., Chadburn, S., Jackson, R. B., Jones, M., MacDonald, G., Marushchak, M., Olefeldt, D., Packalen, M., Siewert, M.  
428 B., Treat, C., Turetsky, M., Voigt, C., and Yu, Z.: Large stocks of peatland carbon and nitrogen are vulnerable to permafrost thaw, *Proc.*  
429 *Natl. Acad. Sci. U. S. A.*, <https://doi.org/10.1073/pnas.1916387117>, 2020.
- 430 Ito, A.: A historical meta-analysis of global terrestrial net primary productivity: Are estimates converging?, *Glob. Chang. Biol.*, 17, 3161–  
431 3175, 2011.
- 432 Jin, D., Hoagland, P., and Buesseler, K. O.: The value of scientific research on the ocean’s biological carbon pump, *Sci. Total Environ.*,  
433 749, 141357, 2020.
- 434 Jones, C. D., Robertson, E., Arora, V., Friedlingstein, P., Shevliakova, E., Bopp, L., Brovkin, V., Hajima, T., Kato, E., Kawamiya, M.,  
435 Liddicoat, S., Lindsay, K., Reick, C. H., Roelandt, C., Segsneider, J., and Tjiputra, J.: Twenty-first-century compatible CO<sub>2</sub> emissions  
436 and airborne fraction simulated by CMIP5 earth system models under four representative concentration pathways, *J. Clim.*, 26, 4398–  
437 4413, 2013.
- 438 Kaplan, J. O., Krumhardt, K. M., and Zimmerman, N. E.: The effects of land use and climate change on the carbon cycle of Europe over  
439 the past 500 years, *Glob. Chang. Biol.*, 18, 902–914, 2012.
- 440 Kawamiya, M., Hajima, T., Tachiiri, K., Watanabe, S., and Yokohata, T.: Two decades of Earth system modeling with an emphasis on  
441 Model for Interdisciplinary Research on Climate (MIROC), *Progress in Earth and Planetary Science*, 7, 1–13, 2020.
- 442 Kriegl, E.: Imprecise probability analysis for integrated assessment of climate change, Verlag nicht ermittelbar, 2005.
- 443 Leach, N. J., Jenkins, S., Nicholls, Z., Smith, C. J., Lynch, J., Cain, M., Walsh, T., Wu, B., Tsutsui, J., and Allen, M. R.: FaIRv2.0.0: a  
444 generalized impulse response model for climate uncertainty and future scenario exploration, *Geosci. Model Dev.*, 14, 3007–3036, 2021.
- 445 Lu, D. and Ricciuto, D.: Efficient surrogate modeling methods for large-scale Earth system models based on machine-learning techniques,  
446 *Geoscientific Model Development*, 12, 1791–1807, 2019.
- 447 Malhi, Y., Phillips, O. L., Cramer, W., Bondeau, A., Schaphoff, S., Lucht, W., Smith, B., and Sitch, S.: Tropical forests and the global  
448 carbon cycle: impacts of atmospheric carbon dioxide, climate change and rate of deforestation, *Philos. Trans. R. Soc. Lond. B Biol. Sci.*,  
449 359, 331–343, 2004.
- 450 Meinshausen, M., Raper, S. C. B., and Wigley, T. M. L.: Emulating coupled atmosphere-ocean and carbon cycle models with a simpler  
451 model, *MAGICC6 – Part 1: Model description and calibration*, *Atmos. Chem. Phys.*, 11, 1417–1456, 2011.
- 452 Meinshausen, M., Vogel, E., Nauels, A., Lorbacher, K., Meinshausen, N., Etheridge, D. M., Fraser, P. J., Montzka, S. A., Rayner, P. J.,  
453 Trudinger, C. M., Krümmel, P. B., Beyerle, U., Canadell, J. G., Daniel, J. S., Enting, I. G., Law, R. M., Lunder, C. R., O’Doherty, S.,  
454 Prinn, R. G., Reimann, S., Rubino, M., Velders, G. J. M., Vollmer, M. K., Wang, R. H. J., and Weiss, R.: Historical greenhouse gas  
455 concentrations for climate modelling (CMIP6), *Geoscientific Model Development*, 10, 2057–2116, 2017.
- 456 Morice, C. P., Kennedy, J. J., Rayner, N. A., Winn, J. P., Hogan, E., Killick, R. E., Dunn, R. J. H., Osborn, T. J., Jones, P. D., and  
457 Simpson, I. R.: An updated assessment of near-surface temperature change from 1850: The HadCRUT5 data set, *J. Geophys. Res.*, 126,  
458 <https://doi.org/10.1029/2019jd032361>, 2021.
- 459 Nelder, J. A. and Mead, R.: A simplex method for function minimization, *Comput. J.*, 7, 308–313, 1965.
- 460 Nicholls, Z., Meinshausen, M., Lewis, J., Corradi, M. R., Dorheim, K., Gasser, T., Gieseke, R., Hope, A. P., Leach, N. J., McBride, L. A.,  
461 Quilcaille, Y., Rogelj, J., Salawitch, R. J., Samset, B. H., Sandstad, M., Shiklomanov, A., Skeie, R. B., Smith, C. J., Smith, S. J., Su, X.,

462 Tsutsui, J., Vega-Westhoff, B., and Woodard, D. L.: Reduced Complexity Model Intercomparison Project Phase 2: Synthesizing Earth  
463 System Knowledge for Probabilistic Climate Projections, *Earths Future*, 9, e2020EF001900, 2021.

464 Nicholls, Z. R. J., Meinshausen, M., Lewis, J., Gieseke, R., Dommenges, D., Dorheim, K., Fan, C.-S., Fuglested, J. S., Gasser, T.,  
465 Golüke, U., Goodwin, P., Hartin, C., Hope, A. P., Krieglner, E., Leach, N. J., Marchegiani, D., McBride, L. A., Quilcaille, Y., Rogelj, J.,  
466 Salawitch, R. J., Samset, B. H., Sandstad, M., Shiklomanov, A. N., Skeie, R. B., Smith, C. J., Smith, S., Tanaka, K., Tsutsui, J., and Xie,  
467 Z.: Reduced Complexity Model Intercomparison Project Phase 1: introduction and evaluation of global-mean temperature response,  
468 *Geosci. Model Dev.*, 13, 5175–5190, 2020.

469 Nijssen, F. J. M. M., Cox, P. M., and Williamson, M. S.: Emergent constraints on transient climate response (TCR) and equilibrium climate  
470 sensitivity (ECS) from historical warming in CMIP5 and CMIP6 models, *Earth Syst. Dyn.*, 11, 737–750, 2020.

471 Ou, Y., Iyer, G., Clarke, L., Edmonds, J., Fawcett, A. A., Hultman, N., McFarland, J. R., Binsted, M., Cui, R., Fyson, C., Geiges, A.,  
472 Gonzales-Zuñiga, S., Gidden, M. J., Höhne, N., Jeffery, L., Kuramochi, T., Lewis, J., Meinshausen, M., Nicholls, Z., Patel, P., Ragnauth,  
473 S., Rogelj, J., Waldhoff, S., Yu, S., and McJeon, H.: Can updated climate pledges limit warming well below 2°C?, *Science*, 374, 693–695,  
474 2021.

475 Pennington, S. and Vernon, C.: HectorUI: An Interactive Climate Model, IN33B–05, 2021.

476 Pressburger, L. and Dorheim, K. R.: JGCRI/hector\_cmip6data: v1.0, <https://doi.org/10.5281/zenodo.7304553>, 2022.

477 Pressburger, L., Dorheim, K., Keenan, T., McJeon, H., Smith, S., and Bond-Lamberty, B.: Quantifying airborne fraction trends and the  
478 destination of anthropogenic CO<sub>2</sub> by tracking carbon flows in a simple climate model, *Environ. Res. Lett.*, in press, 2023.

479 R Core Team: R: A Language and Environment for Statistical Computing v4.1.0, R Foundation for Statistical Computing, Vienna, Austria,  
480 2021.

481 Sarofim, M. C., Smith, J. B., St Juliana, A., and Hartin, C.: Improving reduced complexity model assessment and usability, *Nat. Clim.*  
482 *Chang.*, 11, 1–3, 2021.

483 Schädel, C., Schuur, E. A. G., Bracho, R., Elberling, B., Knoblauch, C., Lee, H., Luo, Y., Shaver, G. R., and Turetsky, M. R.: Circumpolar  
484 assessment of permafrost C quality and its vulnerability over time using long-term incubation data, *Glob. Chang. Biol.*, 20, 641–652, 2014.

485 Schwarber, A. K., Smith, S. J., Hartin, C. A., Vega-Westhoff, B. A., and Sriver, R.: Evaluating climate emulation: fundamental impulse  
486 testing of simple climate models, *Earth Syst. Dynam.*, 10, 729–739, 2019.

487 Smith, C., Nicholls, Z. R. J., Armour, K., Collins, W., Forster, P., Meinshausen, M., Palmer, M. D., and Watanabe, M.: The Earth’s  
488 Energy Budget, Climate Feedbacks, and Climate Sensitivity Supplementary Material, in: *Climate Change 2021: The Physical Science*  
489 *Basis. Contribution of Working Group I to the Sixth Assessment Report of the Intergovernmental Panel on Climate Change*, edited by:  
490 Masson-Delmotte, V., Zhai, P., Pirani, A., Connors, S. L., Péan, C., Berger, S., Caud, N., Chen, Y., Goldfarb, L., Gomis, M. I., Huang, M.,  
491 Leitzell, K., Lonnoy, E., Matthews, J. B. R., Maycock, T. K., Waterfield, T., Yelekçi, O., Yu, R., and Zhou, B., 2021.

492 Smith, C. J., Kramer, R. J., Myhre, G., Forster, P. M., Soden, B. J., Andrews, T., Boucher, O., Faluvegi, G., Fläschner, D., Hodnebrog, Ø.,  
493 Kasso, M., Kharin, V., Kirkevåg, A., Lamarque, J.-F., Mühlenthal, J., Olivie, D., Richardson, T., Samset, B. H., Shindell, D., Stier, P.,  
494 Takemura, T., Voulgarakis, A., and Watson-Parris, D.: Understanding Rapid Adjustments to Diverse Forcing Agents, *Geophys. Res. Lett.*,  
495 45, 12,023–12,031, 2018.

496 Takahashi, T., Sutherland, S. C., Wanninkhof, R., Sweeney, C., Feely, R. A., Chipman, D. W., Hales, B., Friederich, G., Chavez, F.,  
497 Sabine, C., Watson, A., Bakker, D. C. E., Schuster, U., Metzl, N., Yoshikawa-Inoue, H., Ishii, M., Midorikawa, T., Nojiri, Y., Körtzinger,  
498 A., Steinhoff, T., Hoppema, M., Olafsson, J., Arnarson, T. S., Tilbrook, B., Johannessen, T., Olsen, A., Bellerby, R., Wong, C. S., Delille,  
499 B., Bates, N. R., and de Baar, H. J. W.: Climatological mean and decadal change in surface ocean pCO<sub>2</sub>, and net sea–air CO<sub>2</sub> flux over the  
500 global oceans, *Deep Sea Res. Part 2 Top. Stud. Oceanogr.*, 56, 554–577, 2009.

501 Tanaka, K., Krieglner, E., Bruckner, T., Hooss, G., Knorr, W., Raddatz, T. J., and Tol, R.: Aggregated carbon cycle, atmospheric chemistry,  
502 and climate model (ACC2), Institute, Max Planck, Hamburg, 188 pp., 2007.

503 Thornton, P. E. and Rosenbloom, N. A.: Ecosystem model spin-up: Estimating steady state conditions in a coupled terrestrial carbon and  
504 nitrogen cycle model, *Ecol. Modell.*, 189, 25–48, 2005.

505 Vega-Westhoff, B., Sriver, R. L., Hartin, C. A., Wong, T. E., and Keller, K.: Impacts of observational constraints related to sea level on  
506 estimates of climate sensitivity, *Earths Future*, 7, 677–690, 2019.

507 Wang, S., Zhang, Y., Ju, W., Chen, J. M., Ciais, P., Cescatti, A., Sardans, J., Janssens, I. A., Wu, M., Berry, J. A., Campbell, E.,  
508 Fernández-Martínez, M., Alkama, R., Sitch, S., Friedlingstein, P., Smith, W. K., Yuan, W., He, W., Lombardozzi, D., Kautz, M., Zhu, D.,  
509 Lienert, S., Kato, E., Poulter, B., Sanders, T. G. M., Krüger, I., Wang, R., Zeng, N., Tian, H., Vuichard, N., Jain, A. K., Wiltshire, A.,  
510 Haverd, V., Goll, D. S., and Peñuelas, J.: Recent global decline of CO<sub>2</sub> fertilization effects on vegetation photosynthesis, *Science*, 370,  
511 1295–1300, 2020.

512 Willner, S., Hartin, C., and Gieseke, R.: pyhector: A Python interface for the simple climate model Hector, *J. Open Source Softw.*, 2, 248,  
513 2017.

514 Winkler, K., Fuchs, R., Rounsevell, M., and Herold, M.: Global land use changes are four times greater than previously estimated, *Nat.*  
515 *Commun.*, 12, 2501, 2021.

516 Woodard, D. L., Shiklomanov, A. N., Kravitz, B., Hartin, C., and Bond-Lamberty, B.: A permafrost implementation in the simple carbon-  
517 climate model Hector v.2.3pf, *Geosci. Model Dev.*, 14, 4751–4767, 2021.

518 Yue, C., Ciais, P., Houghton, R. A., and Nassikas, A. A.: Contribution of land use to the interannual variability of the land carbon cycle,  
519 *Nat. Commun.*, 11, 3170, 2020.

520 Zeebe, R. E. and Wolf-Gladrow, D.: *CO<sub>2</sub> in Seawater: Equilibrium, Kinetics, Isotopes*, Gulf Professional Publishing, 346 pp., 2001.

521



522 **Table 1. Default Hector parameter values and their sources.** The parameter name column is the name as it appears in the  
523 model's ini (initialization) files. This is not an exhaustive table of Hector parameters but rather contains the parameters that  
524 have been updated since Hartin et al. (2015). For a complete collection of parameter values and their sources, refer to the  
525 default initialization files available at <https://github.com/JGCRI/hector/tree/main/inst/input>. Preindustrial values here are  
526 assumed to be circa 1745, the start of a Hector run.

Parameter	Description	Value	Units	Source
CH4N	Natural CH <sub>4</sub> Emissions are assumed to be constant over the historical and future period	338	Tg CH <sub>4</sub> yr <sup>-1</sup>	See section 2.2.6 for details
N2ON	Natural N <sub>2</sub> O emissions, assumed to be constant of the historical and future period	9.7	Tg N yr <sup>-1</sup>	
beta	CO <sub>2</sub> fertilization factor ( $\beta$ ) (increase in NPP productivity with increasing CO <sub>2</sub> concentrations)	0.55	unitless	
q10_rh	Heterotrophic respiration temperature sensitivity factor ( $Q_{10}$ )	2.2	unitless	
diff	Vertical ocean heat diffusivity ( $\kappa$ ), the rate of heat diffuses into the ocean	1.16	cm <sup>2</sup> /s	
preind_surface_c	Initial size of the preindustrial surface ocean carbon pool	900	Pg C	Figure 5.12 (Canadell et al., 2021)
preind_interdeep_c	Initial size of the preindustrial intermediate and deep ocean carbon pool	37100	Pg C	
C0	Preindustrial CO <sub>2</sub> concentration	277.15	ppmv CO <sub>2</sub>	Table 7.SM.1 (Smith et al., 2021)
N0	Preindustrial N <sub>2</sub> O concentration	273.87	ppbv N <sub>2</sub> O	
M0	Preindustrial CH <sub>4</sub> concentration	731.41	ppbv CH <sub>4</sub>	
npp_flux0	Preindustrial net primary production	56.2	Pg C yr <sup>-1</sup>	Ito (2011)
TOS0	Mean preindustrial absolute ocean air temperature	18	°C	

deltaHL0	Difference between high latitude preindustrial ocean temp and TOS0	-16.4	°C	From processed CMIP6 data (Pressburger and Dorheim, 2022)
deltaLL0	Difference between low latitude preindustrial ocean temp and TOS0	2.9	°C	

527

**Table 2: Descriptions and summaries of the Hector constraints.** The constraint name column reflects the name as it appears in the model's ini (initialization) files.

Name	Description	Implementation
CO2_constrain	Time series of CO <sub>2</sub> concentration values (ppmv CO <sub>2</sub> )	CO <sub>2</sub> radiative forcing (RF) is calculated from the user-provided CO <sub>2</sub> concentrations and then used to calculate total RF and temperature. If needed, CO <sub>2</sub> is debited/credited to/from the deep ocean to meet the CO <sub>2</sub> concentration constraint and satisfy Hector's global carbon cycle mass balance check.
CH4_constrain	Time series of CH <sub>4</sub> concentration values (ppbv CH <sub>4</sub> )	CH <sub>4</sub> RF is calculated from the user-provided CH <sub>4</sub> concentrations, feeding into total RF and temperature.
N2O_constrain	Time series of N <sub>2</sub> O concentration values (ppbv N <sub>2</sub> O)	N <sub>2</sub> O RF is calculated from the user-provided N <sub>2</sub> O concentrations.
X_constrain  (X is the identifier for one of 26 halocarbons modeled by Hector)	Time series for a single halocarbon concentration (pptv)	RF for halocarbon X is calculated from the user-provided concentrations.
RF_tot_constrain	Time series of total radiative forcing value (W m <sup>-2</sup> )	User-provided total RF values are used to calculate temperature and heat flux. In this case, the emission inputs do not drive model behavior.
NBP_constrain	Time series of Net Biome Production values (Pg C yr <sup>-1</sup> )	User-provided NBP values are used to up/downscale NPP and RH so that their total matches the constraint. This effectively bypasses the model's terrestrial carbon cycle.
tas_constrain	Time series of global mean air temperature values (°C)	User-provided temperature values overwrite Hector's, with a smooth transition between the constrained and free-running behavior.

530 **Table 3. Key emergent climate metrics, historical warming, effective radiative forcing, and future warming from**  
531 **Hector versus the IPCC AR6 ‘best estimates’ from the AR6 Table 7.SM.4.** The Hector values were generated from runs  
532 using Hector's default parameterization in the free-running emission-driven mode for historical and SSP scenarios. The  
533 parenthetical IPCC AR6 values indicate the AR6 ‘very likely’ (5-95)% ranges. Acronyms include equilibrium climate  
534 sensitivity (ECS), transient climate response to cumulative carbon emissions (TCRE), transient climate response (TCR),  
535 global surface air temperature (GSAT), and effective radiative forcing (ERF) (Nijssen et al., 2020).

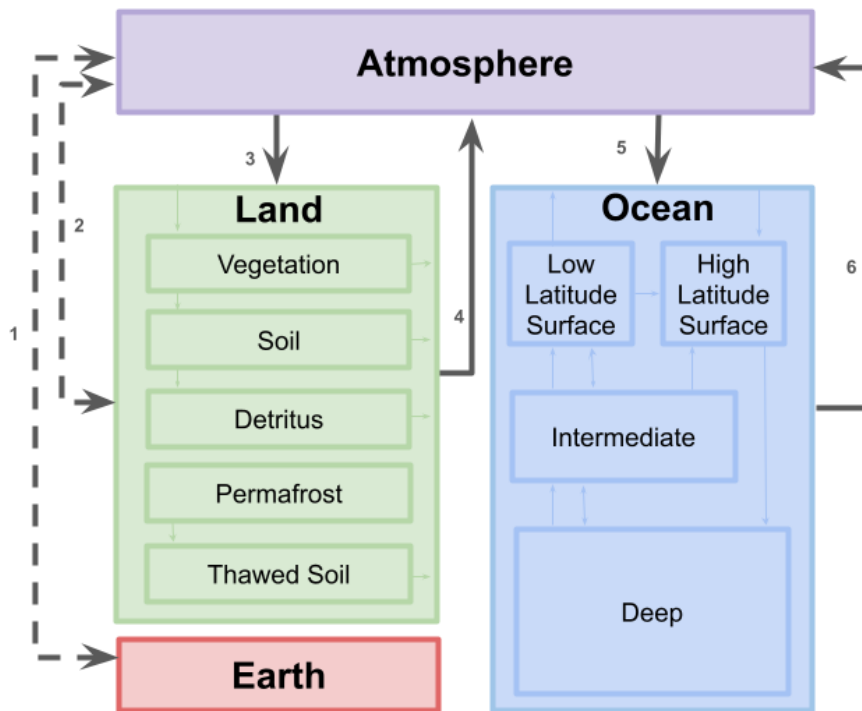
Key Metrics		Hector	IPCC AR6
ECS (°C)		3	3 (2, 5)
TCRE (°C per 1000 GtC)		1.51	1.65 (1, 2.3)
TCR (°C)		1.84	1.8 (1.2, 2.4)
Historical Warming and Effective Radiative Forcing			
GSAT Warming (°C, 1995-2014 relative to 1850-1900)		0.73	0.85 (0.67, 0.98)
Ocean heat content change (ZJ, 1971-2018)		471	396 (329, 463)
Total Aerosol ERF (W m <sup>-2</sup> , 2005-2015 relative to 1750)		-1.24	-1.3 (-2, -0.6)
WMGHG ERF (W m <sup>-2</sup> , 2019 relative to 1750)		3.87	3.32 (3.03, 3.61)
Methane ERF (W m <sup>-2</sup> , 2019 relative to 1750)		0.54	0.54 (0.43, 0.65)
Future Warming (GSAT, °C relative to 1995-2014)			
SSP1-1.19	2021-2040	0.73	0.61 (0.38, 0.85)
	2041-2060	0.90	0.71 (0.4, 1.07)
	2081-2100	0.72	0.56 (0.24, 0.96)
SSP1-2.6	2021-2040	0.75	0.63 (0.41, 0.89)

	2041-2060	1.08	0.88 (0.54, 1.32)
	2081-2100	1.10	0.90 (0.51, 1.48)
SSP2-4.5	2021-2040	0.75	0.66 (0.44, 0.90)
	2041-2060	1.29	1.12 (0.78, 1.57)
	2081-2100	1.98	1.81 (1.24, 2.59)
SSP3-7.0	2021-2040	0.76	0.67 (0.45, 0.92)
	2041-2060	1.43	1.28 (0.92, 1.75)
	2081-2100	2.94	2.76 (2.00, 3.75)
SSP5-8.5	2021-2040	0.88	0.76 (0.51, 1.04)
	2041-2060	1.74	1.54 (1.08, 2.08)
	2081-2100	3.79	3.50 (2.44, 4.82)

536

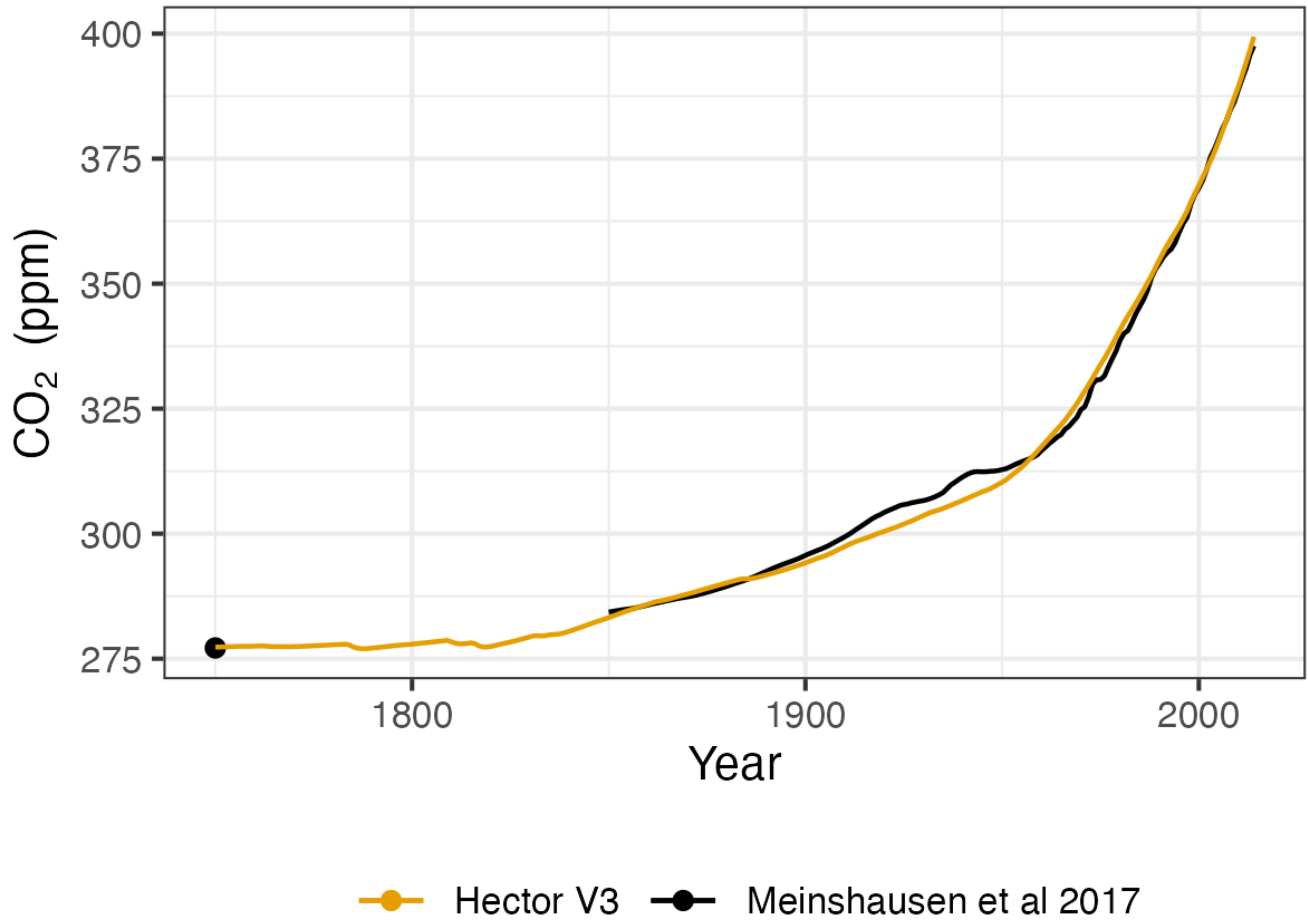
537

538 **Figure 1. Conceptual diagram of the CO<sub>2</sub> fluxes (numbered thick gray arrows) between Hector’s four major carbon**  
 539 **cycle boxes: a well-mixed atmosphere (Atmosphere), terrestrial carbon cycle (Land), ocean carbon cycle (Ocean), and**  
 540 **geological fossil fuel reservoir (Earth).** The thinner arrows within the land and ocean boxes allude to Hector’s more  
 541 complex submodule carbon cycle dynamics, which are not discussed in detail here. The solid lines indicate that CO<sub>2</sub> fluxes  
 542 are calculated within Hector, whereas the dashed lines indicate that the fluxes are externally defined inputs read into the  
 543 model; two-headed arrows imply a potential two-way exchange of carbon. The fluxes are: (1) CO<sub>2</sub> emissions from fossil  
 544 fuels and industry and uptake of carbon capture technologies; (2) CO<sub>2</sub> emissions and uptake from land use change (e.g.,  
 545 afforestation, deforestation, etc.); (3) vegetation uptake from the atmosphere (4) the aggregate CO<sub>2</sub> from respiration from the  
 546 terrestrial biosphere; and ocean carbon (5) uptake and (6) outgassing. The model’s permafrost implementation (Woodard et  
 547 al., 2021) emits both CO<sub>2</sub> and CH<sub>4</sub> into the atmosphere from its “Thawed Soil” pool, whereas the “Soil” pool emits only  
 548 heterotrophic CO<sub>2</sub> respiration.



549  
 550  
 551  
 552

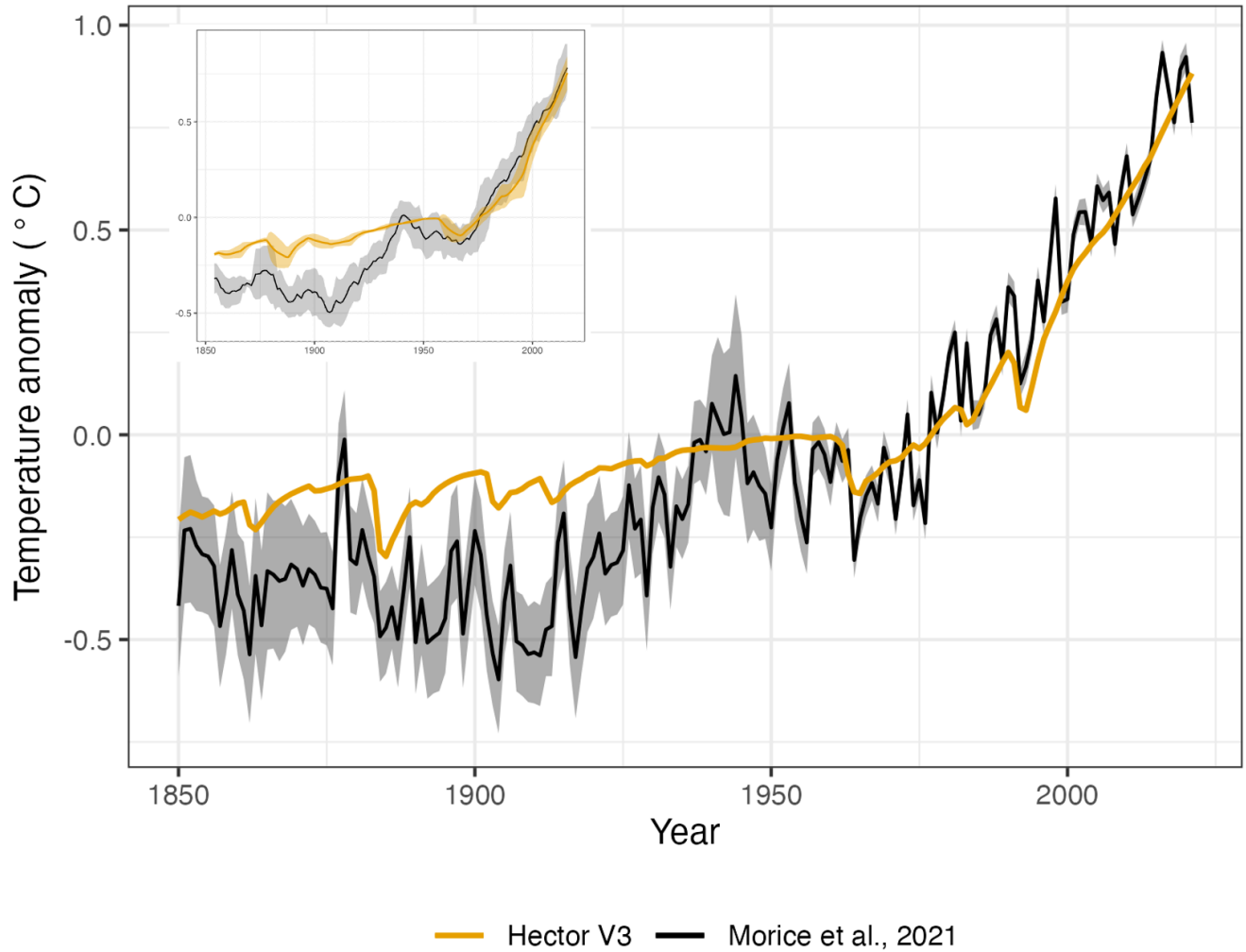
553 **Figure 2. Hector CO<sub>2</sub> concentrations (orange) compared with the CMIP6 (Meinshausen et al., 2017) CO<sub>2</sub>**  
554 **concentrations observational product (black)**



555

556

557 **Figure 3. Global mean surface temperature anomaly relative to 1951-1980 for Hector (orange) and HadCRUT 5**  
558 **global mean surface temperature observations (Morice et al., 2021) (black, with associated uncertainty).** The inset  
559 **figure shows the rolling decadal average.**

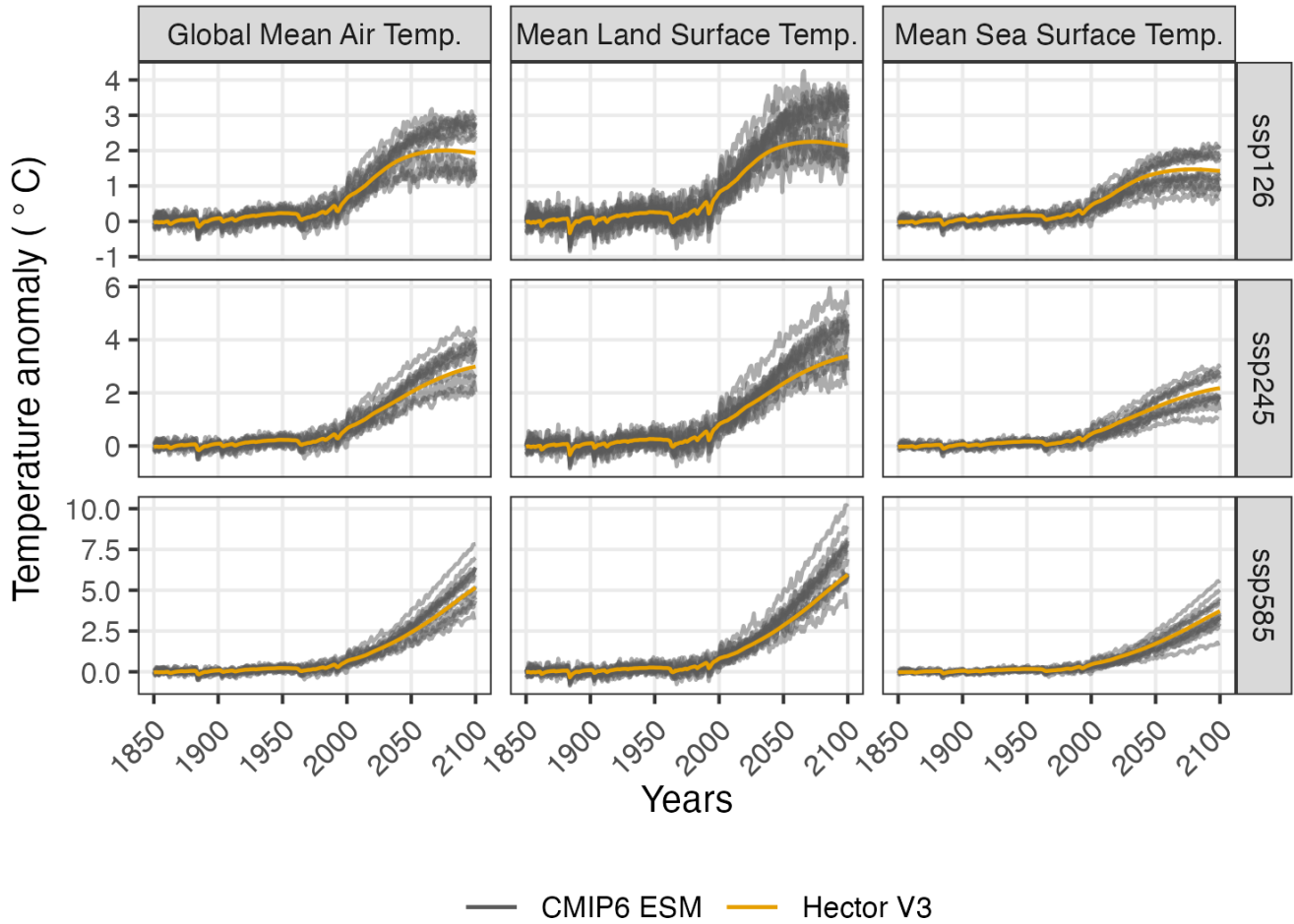


560

561



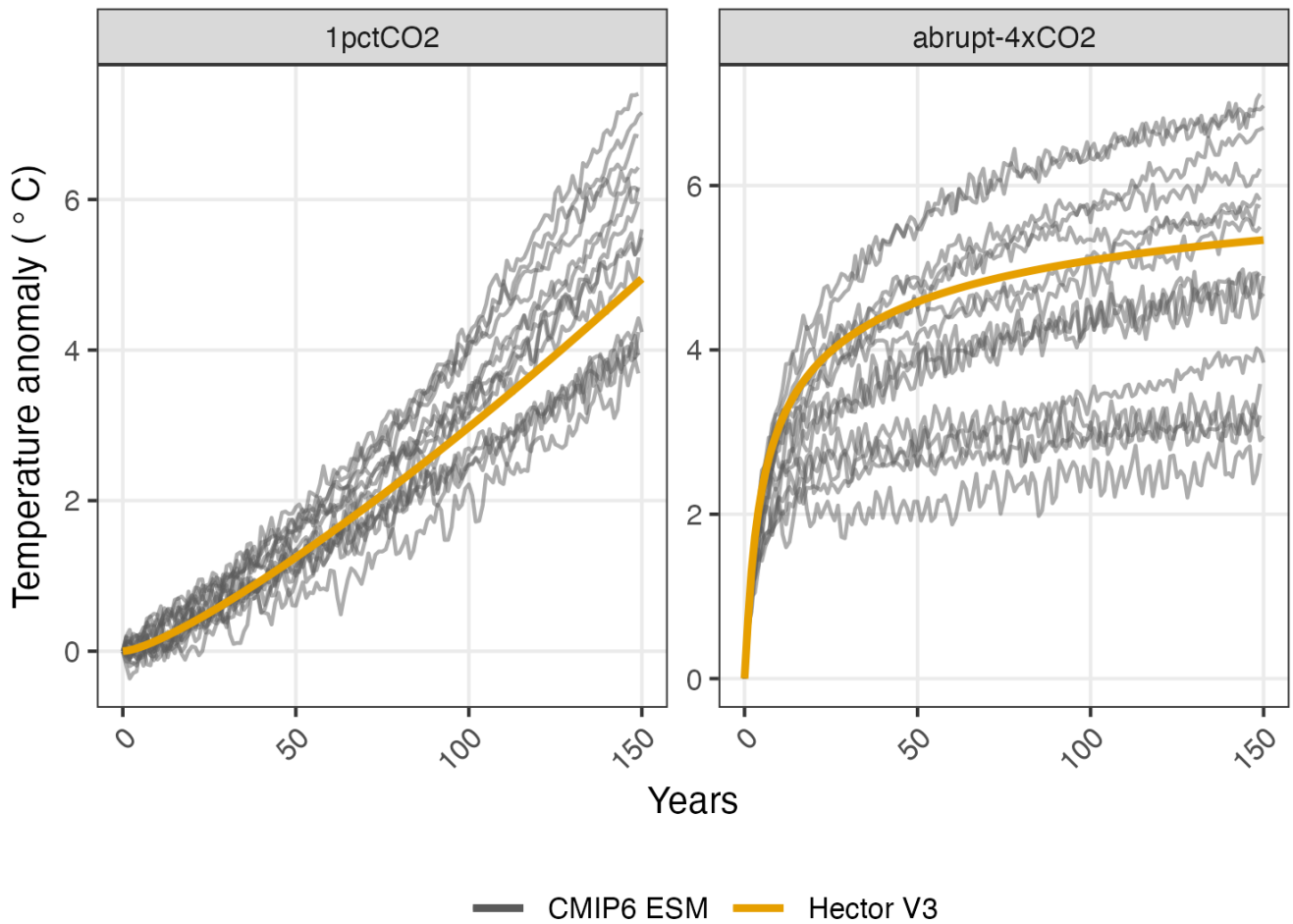
562 **Figure 4. Global, land, and sea surface temperature anomalies relative to 1850-1900 from concentration-driven**  
 563 **(“constrained”) Hector, in orange, and temperature output from 15 different CMIP6-participating ESMs, in grey**  
 564 **(see Supplementary Table 8).**



565

566

567 **Figure 5. Global temperature anomaly from 1% CO<sub>2</sub> and 4xCO<sub>2</sub> stylized experiments (Eyring et al., 2016) for Hector**  
568 **(orange) and 15 different CMIP6 participating ESMs (grey lines; see Supplementary Table 8).**



569